

Corrosion and tribocorrosion behavior of plasma nitrated AA7075 - T651

Leticia Oliveira Rocha¹

Maria Gabriela Galvão Camarinha¹ 

Gislene Valdete Martins²

Ihsan Çaha³ 

Alexandra Alves³ 

Renata Jesuina Takahashi¹ 

Fatih Toptan^{3,4,5} 

Danieli Aparecida Pereira Reis^{1*} 

Abstract

The 7075 aluminum alloy in T651 presents interesting properties in high stressed applications, however, it has low surface properties of hardness and chemical stability. Plasma nitriding is an alternative method of raising surface hardness, fatigue resistance, wear and corrosion of alloys. In this work the corrosion and tribocorrosion behavior of AA7075 - T651 with plasma nitriding treatment were studied in comparison untreated alloy. Corrosion behavior was investigated in 3.5 wt.% NaCl solution at room temperature performing potentiodynamic polarization test and electrochemical impedance spectroscopy. Tribocorrosion behavior was investigated using a ball-on-plate tribometer, against an alumina ball, under 1 N normal load and 1 Hz frequency in 3.5 wt.% NaCl solution at room temperature. The corrosion results showed that both conditions exhibited pitting corrosion that occurred at corrosion potential. The plasma nitrated alloy presented a concentrated and consequently accelerated corrosion process in the fault regions of the layer formed and the formation of a layer of corrosion products that can act as extra protection. The tribocorrosion results for plasma nitrated alloy indicated a slightly more stable behavior, showing no significant changes in the electrochemical potential during the tribocorrosion test, together with a slightly lower volume and rate of wear.

Keywords: 7075-T651 aluminum alloy; Plasma nitriding; Corrosion; Tribocorrosion.

1 Introduction

The aluminum alloys of 7XXX series have zinc (Zn - 1wt.% to 8wt.%), magnesium (Mg - 2.1 wt.% to 2.9 wt.%), and copper (Cu - 1.2 wt.% to 2.0 wt.%) as the main alloying elements giving properties such as high toughness and high mechanical resistance [1-3]. Among the aluminum alloys in this series, there is the AA7075 that can be thermally treated, by precipitation hardening, through the dissolution of alloying elements into the solid solution and subsequent precipitation in the form of submicroscopic particles (artificial aging) to obtain the AA7075-T6 [2-5]. Additional variations in this treatment can be performed for internal stress relieving, like 1-3% traction of the material in its length, obtaining AA7075-T651 condition [3,6]. The AA7075 alloy presents its main applications in the aeronautical sector and in components subject to high

stress [2-4]. Despite the properties, such as high mechanical strength and low density, which make this alloy interesting for these types of applications, it has low surface properties as hardness, wear resistance and thermal and chemical stability [7,8] when compared to other aluminum alloys as AA2024 [9]. These properties become more relevant when subjected to corrosive, tribocorrosive and mechanical conditions, as in the fatigue phenomenon [10-13]. The plasma nitriding of the 7075 aluminum alloy aims to improve its surface properties by introducing an aluminum nitride (AlN) surface layer. This AlN layers has high hardness, wear resistance, corrosion resistance, thermal conductivity (comparable to aluminum) and electrical resistivity, which are very attractive for advanced technological applications, such as in components and aeronautical structures [8].

¹ Laboratório de Comportamento Mecânico de Metais, Instituto de Ciência e Tecnologia, Universidade Federal de São Paulo, UNIFESP, São José dos Campos, SP, Brasil.

² Instituto Tecnológico de Aeronáutica, ITA, São José dos Campos, SP, Brasil.

³ Centro de Sistema Microeletromecânicos, Universidade do Minho, Guimarães, Portugal.

⁴ Departamento de Engenharia Mecânica, Universidade do Minho, Guimarães, Portugal.

⁵ Instituto de Biomateriais, Tribocorrosão e Nanomedicina, Universidade Estadual Paulista, UNESP, Bauri, SP, Brasil.

*Corresponding author: danieli.reis@unifesp.br



Thereby, the objective of the present study was to investigate corrosion and tribocorrosion behavior of the 7075-T651 aluminum alloy after plasma nitriding in comparison with the same alloy without nitriding treatment was studied in the saltwater environment (3.5 wt.% NaCl solution).

2 Materials and method

The corrosion and tribocorrosion tests were performed in cylindrical 7075-T651 aluminum alloy samples ($\varnothing 15.88$ mm and 6 mm of thickness) with and without plasma nitriding treatment. The plasma nitriding treatment was conducted in the Associated Laboratory of Sensors and Materials of the National Institute of Space Research (LABAS/INPE - Brazil) by active screen plasma nitriding technique with a DC power (20 Hz e duty cycle 40). Previous to the nitriding treatment, the samples were cleaned by sputtering with argon and hydrogen at 1:1 ratio (18 sccm:18 sccm). Plasma nitriding was performed at a constant 4:1 nitrogen:hydrogen gas flow ratio (40 sscm:10 sccm), the average temperature was 350 °C, and the average pressure 0.25 torr. The samples without nitriding were prepared for the tests by grinding down to 2500 mesh size SiC paper and polishing with colloidal silica (OP-S 50 nm), 24 hours before each test, while the samples with nitriding did not have the surface prepared. The samples were cleaned in an ultrasonic bath in propanol for 10 minutes and then in distilled water for 5 minutes and stored in a desiccator for 24 hours before corrosion or tribocorrosion tests.

Corrosion tests were performed in a three-electrode electrochemical cell adapted from ASTM: G3-2014 [14] at room temperature. A saturated calomel reference electrode (SCE), Pt counter electrode and a solution of 3.5 wt.% NaCl (electrolyte) were used in the tests. The exposed surface area of the analyzed samples (working electrode) was 0.385 cm². The measurements were performed using a Gamry Instruments Reference 600TM potentiostat, controlled by Gamry Instruments Framework (Gamry Instruments, Warminster, PA, USA) software.

The open circuit potential (OCP) was measured for 30 minutes for the system stabilization, followed by electrochemical impedance spectroscopy (EIS) performed at -20 mV_{OCP} by scanning a range of frequencies from 10⁻² to 10⁵ Hz with a sinusoidal signal of 10 mV.

After EIS measurements, OCP was measured for 10 minutes, and afterwards the potentiodynamic polarization was measured from the cathodic potential (-0.25 V_{OCP}) to the anodic potential (0.3 V_{SCE}) with a scanning rate of 1 mV/s.

Tribocorrosion tests were performed in a reciprocating ball-on-plate tribometer with two electrode set-up using a SCE reference electrode with an exposed area of 1.9 cm². The samples were the working electrode, and 10 mm diameter alumina balls (Ceratec) were the counter body. The total displacement amplitude was 5 mm with 1 Hz of sliding frequency, 1 N normal load (corresponding to maximum

Hertzian contact pressures of 0.45 GPa), and 30 min of sliding time. The OCP was monitored before, during, and after the sliding. The friction coefficient was monitored during the sliding.

After corrosion and tribocorrosion tests, samples were ultrasonically cleaned with the same procedure applied before the tests. All tested samples were analyzed by optical microscopy (Leica DM 2500M) before and after the corrosion tests. The worn samples were analyzed scanning electron spectroscopy (SEM, FEI Nova 200) equipped with EDAX energy dispersive X-ray spectroscopy (EDS). All worn surface images were taken as parallel to the sliding direction by using backscattered (BSE) and secondary electron (SE) detector signals. Total wear volume loss was calculated by considering three 2D profiles taken from each wear track (3 measures) using a noncontact profiler (Veeco Dektak) and following the calculation given by Doni et al. [15].

All tests were performed in triplicate for each group to ensure repeatability, and all results were given as the arithmetic mean \pm standard deviation.

3 Results and discussion

3.1 Corrosion tests

3.1.1 OCP and potentiodynamic polarization

The evolution of OCP with the immersion time for AA7075-T651 plasma nitrided and untreated samples is presented in Figure 1A. The oscillations of the potential give an indication of the formation of pits that occur in contact with the electrolyte [16]. The electrochemical potential of the untreated aluminum alloy was slightly more positive than observed for the plasma nitrided alloy. It could indicate a lower corrosion tendency for the untreated alloy, with the E_{OCP} value being approximately -0.71 V_{SCE} for alloy without plasma nitriding treatment and -0.85 V_{SCE} for the alloy with plasma nitriding treatment.

The representative potentiodynamic polarization curves for plasma nitrided and untreated AA7075-T651 alloys are presented in Figure 1B. The polarization curves showed two zones, the cathodic domain below the corrosion potential (E_{corr}), the E_{corr}, and the anodic domain above the E_{corr}. Both alloys presented pitting corrosion occurring at the corrosion potential (E_{corr}), characterized by the plateau created with the increase of the current at a constant potential [17]. The E_{corr} and the pitting potential (E_{pit}) values are -700 ± 1 and -800 ± 5 for AA7075-T651 and AA7075-T651 nitrided, respectively, which shows a slightly more positive potential value for the untreated alloy, indicating the occurrence of pits at a slightly more positive potential. However, the potentiodynamic polarization curve in the case of plasma nitrided alloy is slightly shifted to lower current densities, indicating a slightly lower corrosion kinetics, and corrosion resistance when compared with untreated alloy.

The corrosion resistance of a commercial aluminum alloy (purity of ~99.6%) nitrided using the active plasma nitriding technique ($N_2:H_2=3:1$, 550 °C, com 2.5 h, 5 h, and 7.5 h of treatment) in relation to the same alloy untreated was investigated by the Yazdani et al. [18] using the potentiodynamic polarization technique in 3.5 wt.% NaCl at room temperature.

The results and analysis obtained by these researchers resemble those obtained in the present study, where the untreated alloy achieved a more positive potential (-700mV_{SCE} and -800mV_{SCE} for plasma nitrided and untreated alloy, respectively), indicated by analyzing the potential it cannot be started that higher corrosion resistance instead should be a lower tendency to corrosion. Some of the present authors [11] compared the corrosion behavior of AA70575 after RRA thermal treatment and plasma nitriding. The results showed that the best corrosion behavior was achieved after plasma nitriding treatment once after this treatment, the corrosion current density was reduced compared with untreated alloy. Figure 2 presents optical micrographs of the plasma nitrided and untreated AA7075-T651 alloys, before and after the corrosion tests. It is observed the presence of pits in both alloys after the corrosion test, proving the occurrence of pitting corrosion in both alloys. The presence of microscopic failures/pores/heterogeneities in the superficial layer formed by plasma nitriding in the AA7075-T651 sample (Figure 2C) possibly influenced the corrosion process, with penetration of

the electrolyte to the surface of the aluminum alloy through these failures, which could originate preferential sites for localized corrosion [18].

Schäfer and Stock [19] showed that the 7075-T6 alloy coated with a stoichiometric AlN coating presented higher pitting potential when compared with untreated alloy, leading to good corrosion protection. On the other hand, corrosion protection of the AlN₁ layer is caused by the solubility of AlN₁ in an aqueous solution. On the other hand, McCafferty et al. [20] detected ammonia on corroded AlN_x surfaces, which can explain the corrosion behavior of AlN. Moreover, generally, the corrosion resistance of AlN coatings is significantly affected by the microstructure of the films [21].

3.1.2 Electrochemical impedance spectroscopy

The EIS spectra in the form of a Bode diagram for plasma nitrided and untreated AA7075-T651 alloys are presented in Figure 3. There are two time constants in phase angle form. The first in medium/high frequencies ($10^3 - 10$ Hz) correspond to the resistance (R_{ox}) and capacitance of the oxide (C_{ox}). The second in low frequencies ($10^{-1} - 10^{-2}$ Hz), probably due to the occurrence of localized corrosion, corresponding to the charge transfer resistance (R_{ct}) and capacitance of the double layer (C_{dl}) in this case due to pitting corrosion as already verified by the potentiodynamic polarization curves [15,22].

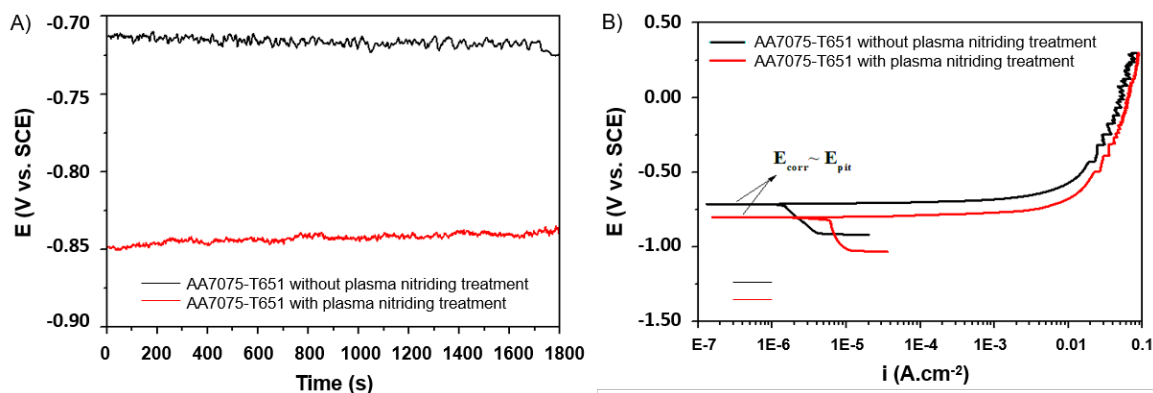


Figure 1. A) OCP evolution with immersion time for plasma nitrided and untreated AA7075-T651 in 3.5 wt% NaCl. B) Potentiodynamic polarization curves of plasma nitrided and untreated AA7075-T651 alloys in 3.5 wt% NaCl solution.

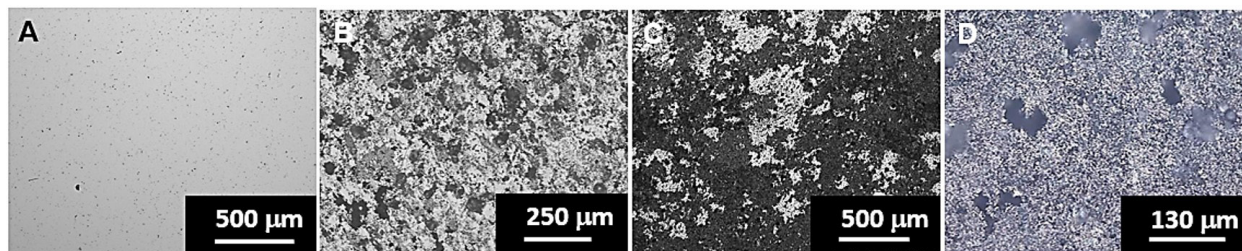


Figure 2. Optical microscopy images of the untreated (A) before and (B) after the corrosion tests and plasma nitrided alloy (C) before and (D) after the corrosion tests.

Regarding the Bode diagram in impedance modulus form ($|Z|$) there are four responses correlated to the resistance of the electrolyte (R_e) in the first plateau in high frequencies ($10^5 - 10^3$ Hz), to the resistance of the oxide layer (R_{ox}) in the first slope in medium frequencies ($10^3 - 10^0$ Hz), to the additional resistance of the electrolyte (R_e') in the second plateau in medium/low frequencies ($10^0 - 10^{-1}$ Hz) and to the resistance of charge transfer in the second slope in low frequencies ($10^{-1} - 10^{-2}$ Hz).

The EIS experimental data were fitted to the EEC using the Echem Analyst Software of Gamry Instruments. The fitting quality was evaluated by its Goodness of fitting (χ^2) value, which presented values below 10^{-3} indicating good correlations between the EEC proposed and the experimental data. The electrical equivalent circuit (EEC) proposed to describe the EIS behavior for plasma nitrided and untreated AA7075-T651 alloys, also already used for other aluminum alloys [16,22], is presented in Figure 4a. Since the resistance of the oxide layer (R_{ox}) tends to be extremely high, not allowing conduction of electrons through the oxide film, normally it is removed from the circuit [16,23], obtaining the circuit presented in Figure 5b that was used for experimental data fitting in this work. The equivalent electrical circuit components are resistance of the electrolyte, R_e ; additional resistance of the electrolyte (inside the failures/pits of de

oxide layer), R_e ; resistance of the oxide layer, R_{ox} ; CPE of the oxide layer, Q_{ox} ; resistance of charge transfer (localized corrosion - pits), R_{ct} ; CPE of the double layer (localized corrosion - pits), Q_{dl} . Since the layer formed in the plasma nitrided alloy is apparently not protective (with the presence of discontinuities) and allows the formation of oxide and pits, as it can be observed through the potentiodynamic polarization curves where $E_{corr} \cong E_{pit}$, the circuit can also be applied to the alloy treated by plasma nitriding.

The EIS spectra fitting parameters values obtained are presented in Table 1. The Q_{ox} and Q_{dl} were converted to a capacitance of the oxide film (C_{ox}) and of the double layer (C_{dl}), respectively, according to Equations 1 and 2, where n = dimensionless coefficient [24].

$$C_{ox} = \left[(Q_{ox} \times Re)^{(1-n)} \right]^{\frac{1}{n}} \tag{1}$$

$$C_{dl} = [Q_{dl} \times (Re + Re')]^{\frac{1}{n}} \tag{2}$$

While, no significant differences were observed for C_{ox} and C_{dl} between the plasma nitrided and untreated alloys, R_{ct} is higher in the case of the plasma nitrided alloy. The difference in R_{ct} values could be related to the area where the corrosion process takes place, with the pits sizes and with the formation of corrosion products. Plasma nitrided alloy presented higher R_{ct} and slightly lower C_{dl} , which indicate that the corrosion process acts in a lower area [15]. Possibly, while on the untreated alloy pitting corrosion process acted on the entire surface of the sample, in the plasma nitrided alloy there was a concentrated and consequently accelerated corrosion process in the regions of the nitride layer discontinuities, which may promote the formation of fewer pits, but with larger dimensions than in the untreated alloy. Furthermore, the higher R_{ct} value observed for the alloy with plasma nitriding treatment possibly occurred due to the formation of a layer of corrosion products that may act as extra protection and somehow block the pits preventing the ion charge transfer [16].

It is observed that the Re and Re' values were practically constant since they are dependent on the distance between

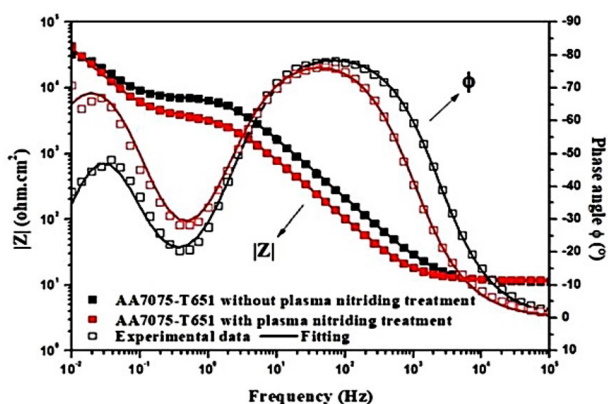


Figure 3. Bode diagram of AA7075-T651 alloys with and without plasma nitriding treatment in 3.5 wt% NaCl solution.

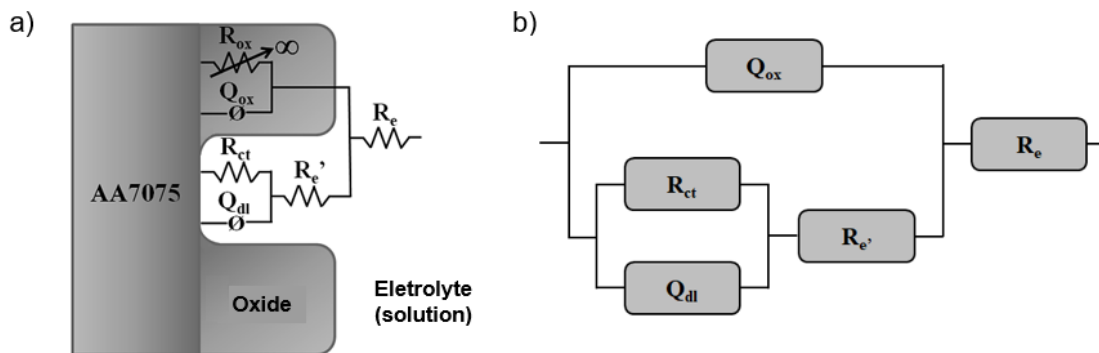
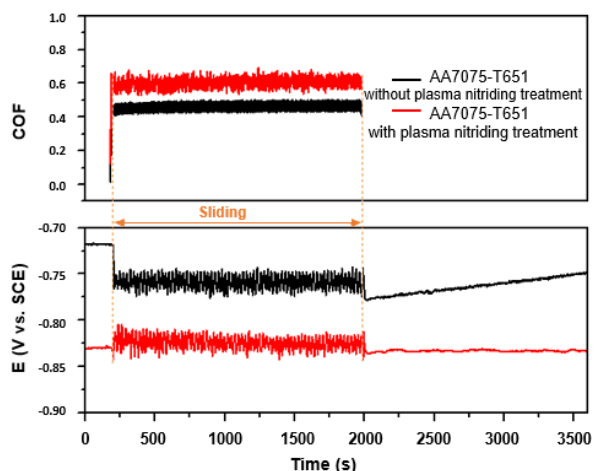


Figure 4. a) Equivalent electrical circuit. b) Equivalent circuit for experimental data fitting.

Table 1. Fitting parameters values for EIS curve

Sample	R_e	R_e'	C_{ox}	n_{ox}	C_{dl}	n_{dl}	R_{ct}
	($\Omega.cm^2$)	($k\Omega.cm^2$)	($\mu F.cm^2$)		($\mu F.cm^2$)		($k\Omega.cm^2$)
AA7075-T651 untreated	12 ± 1	7 ± 4	6 ± 2	0.9	271 ± 104	0.9	37 ± 6
AA7075-T651 plasma nitrided	12 ± 1	5 ± 1	9 ± 3	1	262 ± 54	0.99	244 ± 184

**Figure 5.** Open circuit potential and friction coefficient evolution of plasma nitrided and untreated AA7075-T651 alloys in 3.5 wt% NaCl solution.

the working electrode and the reference electrolyte and the electrolyte concentration [16], which were kept constant during all the tests.

3.2 Tribocorrosion tests

The evolution of OCP before, during and after sliding together with the coefficient of friction (COF) for plasma nitrided and untreated AA7075-T651 alloys are presented in Figure 5. There are three regions in Figure 6, the first one before the mechanical action of sliding, the second one during the sliding and the third one after the sliding.

For both alloys, previously to the mechanical action, the potential corresponds to the stabilization of the system, approximately $-0.72 V_{SCE}$ and $-0.83 V_{SCE}$ for the untreated and plasma nitrided alloy.

The oscillations of the potential observed during the mechanical action give an indication of the formation of pits during the corrosion process [16]. With the interruption of the sliding, it is observed a progressive increase of the potential tending to the initial values corresponding again to the stabilization potential of the alloys.

Regarding the AA7075-T651 alloy with plasma nitriding treatment, it does not present significant changes in the open circuit potential during the tribocorrosion test. This suggests that although the potential of the untreated alloy is slightly more positive (which could indicate a lower tendency for corrosion) than that of the alloy with plasma

nitriding treatment during the entire tribocorrosion test the surface with plasma nitriding treatment promotes a more stable behavior. In relation to the coefficient of friction (COF), it is observed higher values for the alloy with plasma nitriding treatment, which could be correlated with its composition.

During sliding between the contacting surfaces occurs material transfer, where fragments of material detached from the contacting surfaces can accumulate and/or move from one sliding component to the other and could be transferred back to the original surface and/or form wear particles (third bodies) [25-28]. The oscillations of COF are attributed to be caused by the formation and fracture of these wear particles [26]. The plasma nitrided alloy presents higher oscillations during sliding probably due to the higher roughness and also possibly due to the presence of hard nitride particles between the sliding bodies.

3.2.1 Worn surfaces

The SEM micrographs with a detailed view of the wear tracks are presented in Figure 6 for plasma nitrided and untreated AA7075-T651. It is reported in the literature that aluminum alloys and aluminum alloys with nitrided layer present abrasive wear (with the presence of grooves) and plastic deformation [26,29-31]. Parallel grooves can be seen in the sliding direction in both samples.

The grooves of abrasive wear present in the samples probably are caused by the wear particles (debris) formed with the material transfer between the sliding surfaces, which probably are hard oxide particles called “debris” [26,31] and also possibly nitride particles in the case of the samples treated by plasma nitriding. Plastic deformation can also be seen in both samples.

Oxide patches can be seen in both samples (Figure 6), where the sample with plasma nitriding treatment seems to presents a more homogenous distribution of oxide patches than the untreated alloy, what is in accordance with the oxygen percentage in EDS presented in Figure 6C and 6F.

3.2.2 Wear loss

Figure 7 shows the profile obtained with the profilometric characterization of the samples after the tribocorrosion tests, for the untreated and plasma nitrided alloys. The sample with plasma nitriding treatment presented higher roughness as seen in the region out of the wear track ($Z \neq 0$ level).

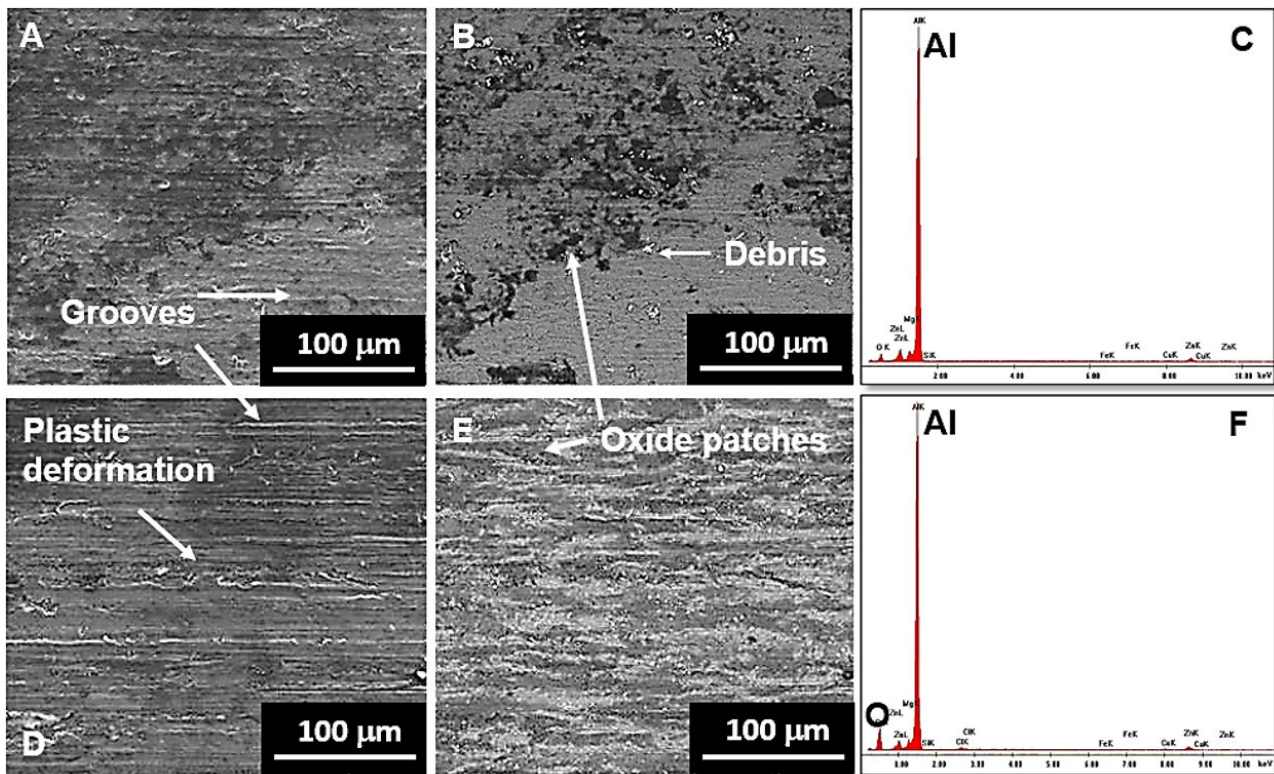


Figure 6. SEM images of the wear tracks for untreated AA7075-T651 alloy by (A) secondary electrons, (B) backscattered electrons and plasma nitrided AA7075-T651 alloy by (C) EDS spectra of the AA7075-T651 alloy untreated (D) secondary electrons, (E) backscattered electrons and (F) EDS spectra of the AA7075-T651 alloy plasma nitrided after tribocorrosion tests.

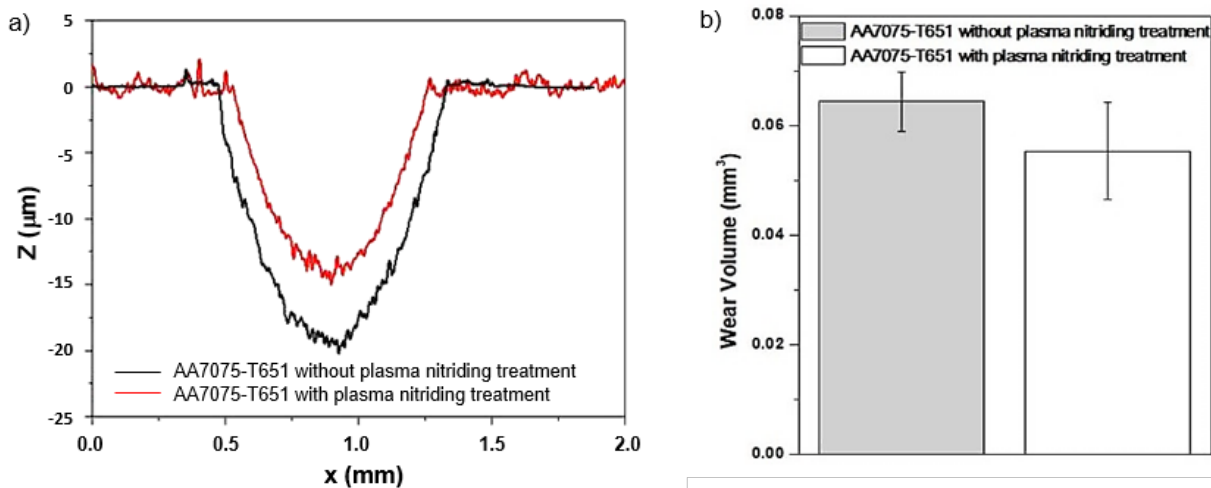


Figure 7. a) Wear profiles of untreated and plasma nitrided AA7075-T651 alloy after tribocorrosion tests. b) Wear volume of AA7075-T651 alloy with and without plasma nitriding treatment after tribocorrosion tests.

Figure 7b present the wear volume determined with profilometry of the wear tracks. Although there are no significant differences, the plasma nitrided alloy presented a slightly lower wear volume (55 ± 8) 10^{-3} mm^3 than the alloy without plasma nitriding treatment (64 ± 5) 10^{-3} mm^3 , as can also be observed in Figure 7a where it shows a slightly

lower depth and width of the wear track, which may indicate a slightly greater behavior.

From the wear volume data, it is possible to calculate the wear rate of the untreated and plasma nitrided alloy, using Equation 3, where T_d = wear rate ($\text{mm}^3/\text{N.m}$), V_d = worn volume (mm^3), C = applied load (N) and d = sliding distance

(m) [31]. Taking into account the wear volume of 0.064 mm^3 and 0.055 mm^3 for untreated and plasma nitrided, respectively, the applied load of 1N and the sliding distance of 0.005 m, it is obtained the wear rates of $12.8 \text{ mm}^3/\text{N.m}$ and $11 \text{ mm}^3/\text{N.m}$ for untreated and plasma nitrided alloy, respectively. It is observed that the alloy treated by the nitriding process showed a lower wear rate than the untreated alloy, which may also indicate superior wear resistance for the treated alloy.

$$T_d = \frac{V_d}{C \times d} \quad (3)$$

4 Conclusion

Corrosion and tribocorrosion behavior of the 7075-T651 aluminum alloy after plasma nitriding in comparison with the same alloy without nitriding treatment was studied in 3.5 wt% NaCl solution. Results indicated that the layer formed by the plasma nitriding process did not promote a significant difference in the corrosion and tribocorrosion behavior of the alloy. It can possibly be explained by the presence of microscopic failures/pores/heterogeneities in the superficial layer formed in the AA7075-T651 sample treated by plasma nitriding that probably acted as accentuating the corrosion process with the origination of preferential sites for localized corrosion from which the surface of

the aluminum alloy can be achieved and attacked by the electrolyte. The corrosion results show that both treated and untreated alloys presented pitting corrosion that occurred at the corrosion potential (E_{corr}). The results indicated that the alloy with plasma nitriding treatment showed slightly lower current densities indicating a slightly increment in the corrosion resistance, which might be explained by formation of a layer of corrosion products that could act as extra protection. The tribocorrosion results for the sample with plasma nitriding treatment showed a slightly more stable behavior, not showing significant electrochemical potential changes during the tribocorrosion test, together with a slightly lower volume and rate of wear.

Acknowledgements

This study was supported by FAPESP (Process nº 2015/19846-2 and 2016/26201-0, Foundation for Research Support of the State of São Paulo – FAPESP), FCT with the reference project UID/EEA/04436/2013 and by FEDER funds through the COMPETE 2020 – Programa Operacional Competitividade e Internacionalização (POCI) with the reference project POCI-01-0145-FEDER-006941. A.C. Alves and. F. Toptan are grateful for financial support through the M-ERA-NET/0001/2015 project (FCT).

References

- 1 Brandt DA, Warner JC. Metallurgy fundamentals: ferrous and nonferrous. Illinois: The Goodheart-willcox Company; 2009.
- 2 Moniz BJ. Metallurgy. Illinois: American Technical Publishers; 2007.
- 3 Hatch JE. Aluminum: properties and physical metallurgy. Ohio: American Society for Metals; 1984.
- 4 Pinho JSR, Campanelli LC, Reis DAP. Case study on the failure analysis of turbojet compressor blades. *Tecnologia em Metalurgia, Materiais e Mineração*. 2022;19:e2760. <http://dx.doi.org/10.4322/2176-1523.20222760>.
- 5 Rocha EG, Camarinha MGG, Reis DAP. Análise fractográfica da liga AA 7075-T6 submetida à fadiga na condição de tratamento RRA e nitretada a plasma. *Matéria (Rio de Janeiro)*. 2023;28(1):e20220305. <http://dx.doi.org/10.1590/1517-7076-RMAT-2022-0305>.
- 6 International ASM. ASM Handbook. Vol. 2: Properties and selection: Nonferrous alloys and special-purpose materials. West Conshohocken: ASM International; 1992.
- 7 Dowling NE. Mechanical behaviour of materials: engineering methods for deformation, fracture, and fatigue. EUA: Person Prentice Hall; 2007.
- 8 Moradshahi M, Tavakoli T, Amiri S, Shayeganmehr S. Plasma nitriding of Al alloys by DC glow discharge. *Surface and Coatings Technology*. 2006;201:567-574. <http://dx.doi.org/10.1016/j.surfcoat.2005.12.002>.
- 9 Reis DAP, Couto AA, Domingues NI Jr, Hirschmann AC, Zepka S, Moura C No. Effect of artificial aging on the mechanical properties of an aerospace aluminum Alloy 2024. *Defect and Diffusion Forum*. 2012;326-328;193-198. <http://dx.doi.org/10.4028/www.scientific.net/ddf.326-328.193>.
- 10 Camarinha MGG, Campanelli LC, Barboza MJR, Reis L, Couto AA, Reis DAP. Fatigue behavior of notched and unnotched 7075-T6 aluminum alloy subjected to retrogression and re-aging (RRA) heat treatment and plasma nitriding. *Theoretical and Applied Fracture Mechanics*. 2023;127:104051. <http://dx.doi.org/10.1016/j.tafmec.2023.104051>.
- 11 Savonov GS, Camarinha MGG, Rocha LO, Barboza MJR, Martins GV, Reis DAP. Study of the influence of the RRA thermal treatment and plasma nitriding on corrosion behavior of 7075-T6 aluminum alloy. *Surface and Coatings Technology*. 2019;374:736-744. <http://dx.doi.org/10.1016/j.surfcoat.2019.04.095>.

- 12 Misak HE, Perel VY, Sabelkin V, Mall S. Corrosion fatigue crack growth behavior of 7075-T6 under biaxial tension-tension cyclic loading condition. *Engineering Fracture Mechanics*. 2013;106:38-48. <http://dx.doi.org/10.1016/j.engfracmech.2013.04.004>.
- 13 Huang Y, Ye X, Hu B, Chen L. Equivalent crack size model for pre-corrosion fatigue life prediction of aluminum alloy 7075-T6. *International Journal of Fatigue*. 2016;88:217-226. <http://dx.doi.org/10.1016/j.ijfatigue.2016.03.035>.
- 14 ASTM International. ASTM G3-14: Standard practice for conventions applicable to electrochemical measurements in corrosion testing. West Conshohocken: ASTM International; 2014.
- 15 Doni Z, Alves AC, Toptan F, Rocha LA, Buciumeanu M, Palaghian L, et al. Dry sliding and tribocorrosion behaviour of hot pressed CoCrMo biomedical alloy as compared with the cast CoCrMo and Ti6Al4V alloys. *Materials & Design*. 2013;52:47-57. <http://dx.doi.org/10.1016/j.matdes.2013.05.032>.
- 16 Moreto J, Marino CEB, Bose Filho WW, Rocha LA, Fernandes JCS. SVET, SKP and EIS study of the corrosion behaviour of high strength Al and Al-Li alloys used in aircraft fabrication. *Corrosion Science*. 2014;84:30-41. <http://dx.doi.org/10.1016/j.corsci.2014.03.001>.
- 17 Schafer H, Stock HR. Improving the corrosion protection of aluminium alloys using reactive magnetron sputtering. *Corrosion Science*. 2004;47:953-964. <http://dx.doi.org/10.1016/j.corsci.2003.06.002>.
- 18 Yazdani A, Soltanich M, Aghajani H. Active screen plasma nitriding of Al using an iron cage: characterization and evaluation. *Vacuum*. 2015;122:127-134. <http://dx.doi.org/10.1016/j.vacuum.2015.09.018>.
- 19 Schäfer H, Stock HR. Improving the corrosion protection of aluminium alloys using reactive magnetron sputtering. *Corrosion Science*. 2005;47:953-964. <http://dx.doi.org/10.1016/j.corsci.2003.06.002>.
- 20 McCafferty E, Natishan PM, Hubler GK. Pitting Behavior of Aluminum Ion Implanted with Nitrogen Corrosion. 1997;7(53):556-561. <http://dx.doi.org/10.5006/1.3290287> 19.
- 21 Casaux Y, Dollet A, Sibieude F, Berjoan R. Influence de l'orientation cristalline sur la résistance à l'oxydation de revêtements de AlN: étude in-situ par diffractométrie X. *Journal de Physique IV*. 1998;8:Pr5-249-Pr5-256. <http://dx.doi.org/10.1051/jp4:1998531>.
- 22 Kendig MW, Mansfeld F. AC electrochemical impedance of a model pit. *Journal of the Electrochemical Society*. 1982;129:C318.
- 23 Mansfeld F, Lin S, Kim S, Shih H. Pitting and passivation of Al alloys and Al-based metal matrix composite. *Journal of the Electrochemical Society*. 1990;137:78-82. <http://dx.doi.org/10.1149/1.2086442>.
- 24 Orazem ME, Tribollet B. *Electrochemical impedance spectroscopy*. New York: Wiley; 2008.
- 25 Cristóbal MJ, Figueroa R, Mera L, Pena G. Tribological behaviour of aluminium alloy AA7075 after ion implantation. *Surface and Coatings Technology*. 2012;209:124-130. <http://dx.doi.org/10.1016/j.surfcoat.2012.08.050>.
- 26 Mischler S. Triboelectrochemical techniques and interpretation methods in tribocorrosion: A comparative evaluation. *Tribology International*. 2008;41:573-583. <http://dx.doi.org/10.1016/j.triboint.2007.11.003>.
- 27 Chen LH, Rigney DA. Transfer during unlubricated sliding wear of selected metal systems. *Wear*. 1985;105(1):47-61. [http://dx.doi.org/10.1016/0043-1648\(85\)90005-5](http://dx.doi.org/10.1016/0043-1648(85)90005-5).
- 28 Zhang A, Chena J, Shi W, Liu Z. Study on tribological behaviors of Fe⁺ ion implanted in 2024 aluminum alloy. *Nuclear Instruments & Methods in Physics Research. Section B, Beam Interactions with Materials and Atoms*. 2000;169(1-4):43-47. [http://dx.doi.org/10.1016/S0168-583X\(00\)00014-8](http://dx.doi.org/10.1016/S0168-583X(00)00014-8).
- 29 Szcancoski JC, Foerster CE, Serbena FC, Fitz T, Kreißig U, Richter E, et al. Mechanical and tribological properties of carbon and nitrogen consecutive ion implantation into aluminium. *Surface and Coatings Technology*. 2006;201(3-4):1488-1494. <http://dx.doi.org/10.1016/j.surfcoat.2006.02.016>.
- 30 Mraied H, Cai W. The effects of Mn concentration on the tribocorrosion resistance of Al-Mn alloys. *Wear*. 2017;380-381:191-202. <http://dx.doi.org/10.1016/j.wear.2017.03.017>.
- 31 ASTM International. ASTM G133-05(2016): Standard Test Method for Linearly Reciprocating Ball-on-Flat Sliding Wear. West Conshohocken: ASTM International; 2016.

Received: 26 May 2023

Accepted: 8 Nov. 2023